International Journal of Research in Engineering, Science and Management
Volume-3, Issue-3, March-2020
www.ijresm.com | ISSN (Online): 2581-5792

Fatigue Analyses of GMAW Welds of Thermo-Mechanically Processed 700MC Ultra High Strength Steel

Bunty Tomar
M.Tech. Student, Department of Materials & Metallurgical Engineering, National Institute of Foundry & Forge Technology, Ranchi, India

***Abstract*: In this work a fatigue study was performed on 6 mm thick plates of commercially available modern high strength steel with minimum yield strength of 700 MPa in order to evaluate the influence on fatigue strength of the following factors: stress concentration at weld toe, weld filler rod and welding process method. The weldability is improved by modeling the welding conditions to evaluate and support the extensive analysis of the mechanical and the metallurgical properties of the welds.**

Materials were welded by two pass GMAW process with two different filler wires. All the welds and respective base material went fatigue testing, tensile testing and hardness measurements under two welding conditions: as welded (AW), welds overfill removed by grinding (WR). Fatigue fracture surfaces were investigated for highest and lowest loads tested using scanning electron microscopy. In tensile tests, the strains were measured using digital image correlation (DIC) equipment.

The failures in fatigue and tensile tests occurred in the recrystallized HAZ or at regions of higher stress concentration. The overfill removing by grinding promotes a significant improvement of the fatigue resistance in comparison with the as welded condition. Removing the welds overfill by grinding leads to an increase of fatigue resistance from 300 to 460 MPa, meaning an improvement of about 50%. DIC measurements revealed that in tensile tests the strain localized in the domain of minimum hardness or in domain of higher stress concentration.

***Keywords*: Characteristic curves, Fatigue, GMAW, Ultra-high strength steel.**

1. Introduction

During the last decades, steel industries had developing great efforts in order to produce steels with higher strength and toughness, better weldability, using less expensive elements. Weight reduction in steel structures has been a point of interest due to the environmental aspects and improvement in efficiency. This has led to an increased interest in using high strength steel grades in various applications of steel plates, namely, in building cranes, ships, truck bodies and different other kinds of containers. This has been possible by introducing a thermo-mechanically controlled process (TMCP) which combines controlled rolling with on-line accelerated cooling. The mechanical properties introduced to the steels through this processing route are virtually better than those obtained by heat treating conventionally rolled or forged steel compositions. The microstructures of TMCP steels are greatly refined as compared to those of conventional processed steels, resulting in a significant improvement in strength and toughness [1]. This high strength of TMCP steel provides potential for considerable improvements in performance and reduction in weight, which are of increasing importance in the transport sector, ships, cranes and in vehicles used in the construction industry. As modern examples of steel are very sensitive to cooling rate and possible tempering after cooling [2], which makes TMCP as the leading process for steel production.

Fatigue is a significant cause of most of the failures because cyclic stresses occur in several applications, such as machine components, bridges, ship structures and other constructions. Therefore, fatigue is related to most mechanical material failures in practices [3,4]. The most significant factor determining the resistance to the cyclic loading is the geometry [5,6]. Surface roughness is also an important factor for fatigue loading, because a rough surface provides more possibilities for crack initialization [7,8]. Purity of base material is also a factor in determining fatigue life. Higher heat input promotes formation of coarse inclusions at the vicinity of the weld, which further decreases the fatigue strength. For an example titanium nitride comes into play if titanium is present [9]. As for welded structures, Baptista et al. [10] have subjected stainless steels welded joints to toe grinding having obtained a significant fatigue life gain and pointed out that grinding technique is a simple way to improve the strength of a new structure.

2. Base material characterization

The base material used in this study is micro alloyed high strength steel with fine grained ferritic-bainitic structure produced by thermo-mechanically controlled process. The plate thickness is 6 mm. The chemical composition and the mechanical properties of this high strength steel are indicated in tables 1 and 2, respectively. Figure 1 represents optical and SEM micrographs of the base material.

Table 1
Limits for the chemical composition of the base material (wt.%)

C	Si	Mn	P	S	Al	Nb	V	Ti
<0.12	<0.25	<2.1	<0.02	<0.01	<0.015	<0.091*	<0.201*	<0.151*

* Sum of Nb, V and Ti < 0.22%

Table 2
Mechanical Properties of the base material

Yield strength (min MPa)	Tensile strength (MPa)	Elongation up to rupture, εr (%)	Impact toughness (J@RT)	Impact Toughness (J@-20°C)
700	750-950	13-16	100*	80*

* Charpy V 10 × 10 mm

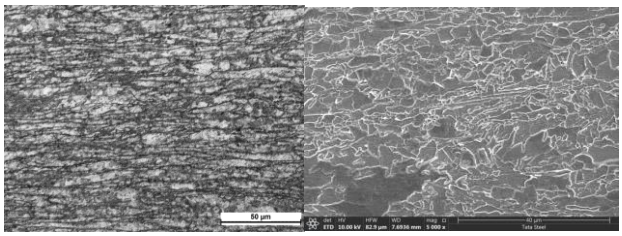

Fig. 1. Optical and SEM micrographs of base material

3. Welding procedure

Material was welded in a two pass using GMAW process with a V shaped grove with a 60° angle and root gap of 1.4 mm between welding specimens. The welding direction was normal to the rolling direction of the base material. Before welding the edges were cut in a guillotine shear machine. To protect the welding process, a combination of 85% of Ar and 15% of CO2 was used, surrounding the arc and the weld. Two different filler wires, ER 120S and ER 70S of 3.2 mm diameter, with the strength of 840 and 490 MPa, respectively, were used for welding. The parameters used during welding were: 216A of current and 20V of voltage with a travel speed of 180 mm/min. The quality of prepared weld joints is tested as per standards of ISO 5817 [11]. The imperfection found in weld joints is negligible and weld joints falls under best weld joints category. Figure 2 presents joint design and welding sequence schematically. All dimensions are in millimeters (mm). Figure 3 presents macrographs of the cross sections of welding conditions with both filler wires.

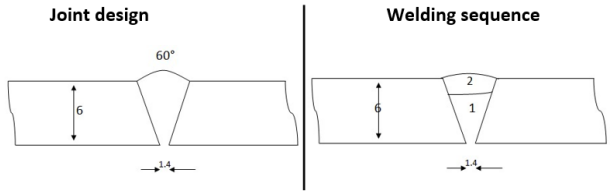

Fig. 2. Schematic presentation of joint design and welding sequence

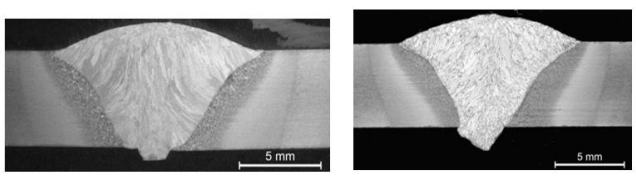

Fig. 3. Macrographs of welds with different filler wires

4. Experimental procedure

In this work, fatigue specimens were prepared in both as welded (AW) and weld overfill removed (WR) conditions for both 120S and 70S filler wire welds. The dimensions and geometry of the specimens in presented in figure 4.

Welded samples were submitted to cyclic loading in Instron 8801 servo-hydraulic testing machine with a load cell of 100 KN. The frequency used in testing was 10 Hz and the stress ratio R was -1. Experimental setup for fatigue is shown in figure 5(a). Five test series were performed in order to analyse the effect of weld toe concentration and welding process for different filler wires: BM, from the base material; 120S AW and 70S AW, in the as welded condition for both filler wires; 120S WR and 70S WR, with overfill removed by grinding respectively.

The fatigue tests were carried out in a load-controlled mode using sinusoidal axial loading with constant amplitude with ambient room temperature in the laboratory. The specimens were tested until their complete failure or to an endurance limit of 2 million cycles if there was no evidence of fatigue cracking. Fatigue results were plotted as S-N curves, presenting the stress range against the number of cycles to fracture. Life was defined as the number of cycles to failure and a total of 36 samples were tested. Fatigue data were statistically analysed according ASTM E739-10 Standard [12]. The DIC equipment was not used during fatigue tests because of very large duration of testing making the capture, storage and processing of these measurements too expensive. Strain fields in fatigue would be compared with the strain fields obtained in the tensile tests, hardness measurements and confirmed with the fractography images.

Tensile tests with digital image correlation (DIC) measurements were also carried out for BM and each welding condition on Instron 8862. The test setup for DIC measurements is presented in figure 5(b). In DIC measurements, 5Hz frequency was used for picturing of specimens. A specific pattern was painted over the specimens and by assessing the change in pattern using VIC2D software, the strain behaviour along with its localization was established.

Hardness maps were generated by measuring hardness of specimens using a Leco LM 247AT micro-hardness tester with an indentation load of 300 grams and dwell time of 13 sec. Measurements were performed along nine lines with a distance of 0.6 mm between all lines and from top and bottom of specimens and with 0.25 mm distance between the points.

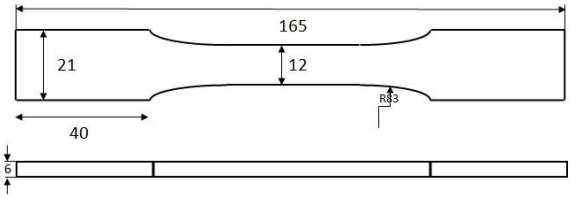

Fig. 4. Dimensions of fatigue test specimens

(a) (b)

Fig. 5. Experimental setup for: a) Fatigue, b) DIC

5. Fatigue test results

A total of 41 specimens were tested: eight specimens for each welding conditions and nine for base material. Fatigue test results and characteristics of load conditions for each specimen are presented in Table 3.

Fatigue test results are presented by S-N curves on a log-log scale in figure 6. Each point represents a value from the experimental test and the fitted lines were obtained by fitting a linear regression Eq. (1) assuming Δσ as the dependent variable.

$$\Delta\sigma = K_0 N_f^{-m} \quad (1)$$

Where Δσ is the stress range, N_f is the number of cycles to failure. The symbols k_0 and m are empirical constants, namely the coefficient and exponent of the S-N curve, respectively. The values for the empirical constants K_0 and m for base material and each welding condition are presented in Table 4.

The overfill removing by grinding performed in the WR specimens promotes a significant improvement of the fatigue resistance in comparison with the as welded (AW) specimens: for a fatigue life of 2 million cycles the stress range is 300 and 460 MPa for 70S AW and 70S WR series, respectively, meaning an improvement of 53% in the fatigue strength. Similarly, for a fatigue life of 2 million cycles the stress range is 300 and 520 MPa for 120S AW and 120S WR series, respectively, meaning an improvement of 73% in the fatigue strength. The exponents of series 120S AW and 70S AW are m=6.03 and m= 6.16, respectively. These lower values of exponent m reveal that crack initiation period of these series is relatively low. Figure 7 displays the crack initiation and crack propagation zones in all welding conditions. It reveals that irrespective of strength of the filler wire used for welding of specimens, less hardness zone and HAZ; in AW conditions crack initiated from the toe of high stress concentration weld overfill. In WR conditions crack initiated from least hardened HAZ and weld zone for 120S and 70S filler wires, respectively. These results could also be compared and confirmed by DIC measurements and hardness maps further.

Table 3
Fatigue test results

Welding condition	Specimen Number	Δσ (MPa)	Number of Cycles	Comments
BM	1	860	35103	
	2	860	39796	
	3	740	142154	
	4	740	154806	
	5	660	672592	
	6	660	856402	
	7	620	1256192	
	8	620	1324922	
	9	540	2000000	Infinite Life
120S AW	1	700	14815	
	2	700	11951	
	3	620	44355	
	4	540	120420	
	5	540	556189	
	6	380	169506	
	7	380	639980	
	8	300	2000000	Infinite Life
70S AW	1	700	16004	
	2	700	17638	
	3	620	52360	
	4	540	104792	
	5	540	491137	
	6	380	702608	
	7	380	921533	
	8	300	2000000	Infinite Life
70S WR	1	700	51438	
	2	700	56725	
	3	660	92508	
	4	620	186402	
	5	520	892322	
	6	520	1538936	Base Material
	7	520	1117605	
	8	460	2000000	Infinite Life
120S WR	1	700	67619	
	2	700	93414	
	3	660	156463	
	4	640	315841	
	5	600	849775	
	6	600	988929	
	7	520	1562320	
	8	520	2000000	Base Material Infinite Life

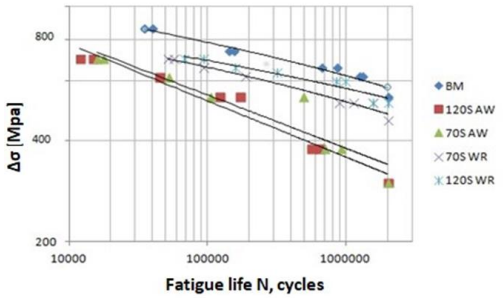

Fig. 6. S-N curves of fatigue test results

Table 4
Values for empirical constants m and K_0

Welding condition	m	K_0
BM	11.15	1.8E37
120S AW	6.03	2.8E21
70S AW	6.16	8.6E21
70S WR	10.35	1.5E34
120S WR	11.08	3.2E36

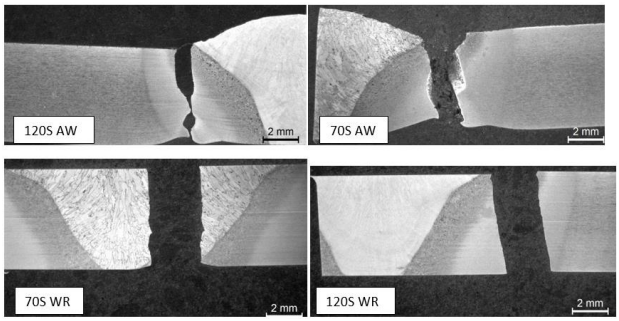

Fig. 7. Fatigue crack initiation and propagation

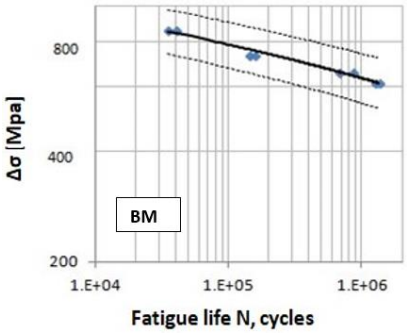

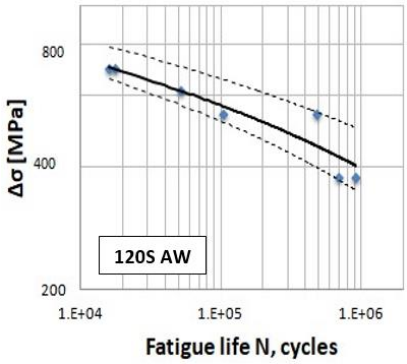

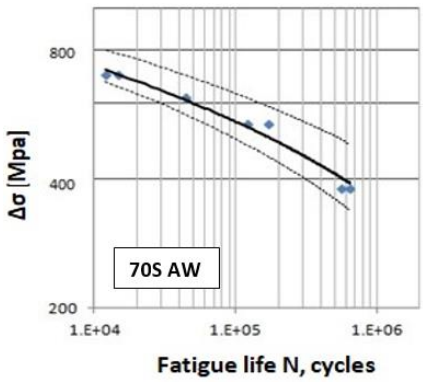

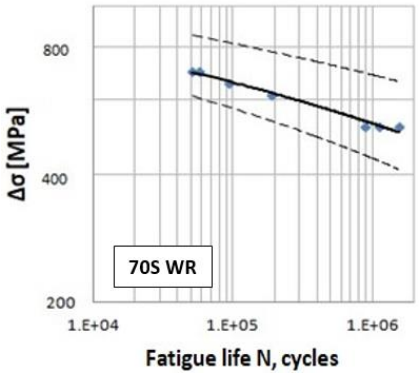

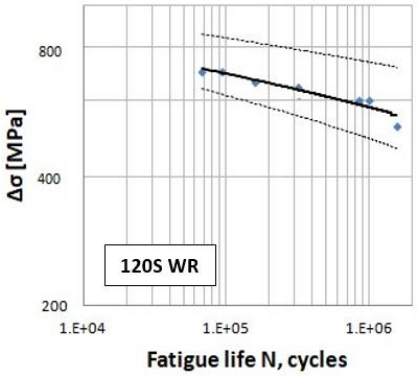

Fig. 8. Curves from the fatigue test results in 95% confidence bands

Figure 8 displays the results of the statistical analysis for 95% confidence bands for fatigue test results carried out using standard E739-91 for base material and each welding condition.

Figure 9 presents images of fracture surfaces: one with the lowest number of cycles and another with highest number of cycles for each welding condition. The crack initiation zone, the propagation zone and the final rupture zone are clearly visible in each specimen. In AW condition, at lower number of cycles the fracture is more like tearing failure with crack initiating along with complete weld toe and rupture with relatively large number of dimples. For higher fatigue life, crack initiated from the edge of weld at face side. In WR condition, crack initiated at the root side in least hardened zone as shown in figure 7 previously. At higher cycles, it can be seen that crack initiated mostly from the weld flaws.

It can be noted, that the main difference between the specimens with the lowest and highest number of cycles is the relative size of the crack propagation zone. It can be concluded from figure 9. This confirms that the propagation stage is the most critical stage in determining the fatigue life of any specimen going under cyclic loading. Figure 10 presents an SEM image showing the propagation zone of 120S AW (N = 639980, Δσ =380 MPa) sample. Fatigue striations, direction of crack propagation and secondary cracking can be recognized from the figure 10.

6. DIC Measurements

To support the fatigue crack initiation observations, DIC

measurement was performed to analyze the localisation of the strain during the tensile testing. A summary of DIC results is presented in figure 11. The images were taken at a frequency of 5 Hz. The shown images have been taken at two points for each weld condition, namely at the ultimate tensile stress and the point just before the fracture. In AW conditions, the strain is localizing in the domain of high concentration at the interface of weld and HAZ. In WR conditions, for 120S AW, the strain localizes in the weakest recrystallized HAZ whereas, for 70S AW, strain localization is occurring in the least hardened weld zone.

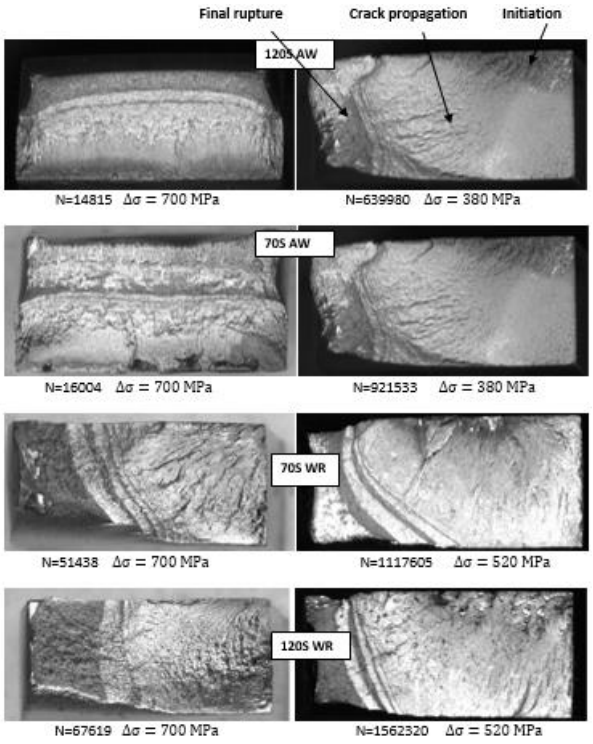

Fig. 9. Fracture surfaces of the specimens with the lowest and the highest number of cycles within each welding condition

7. Hardness measurements

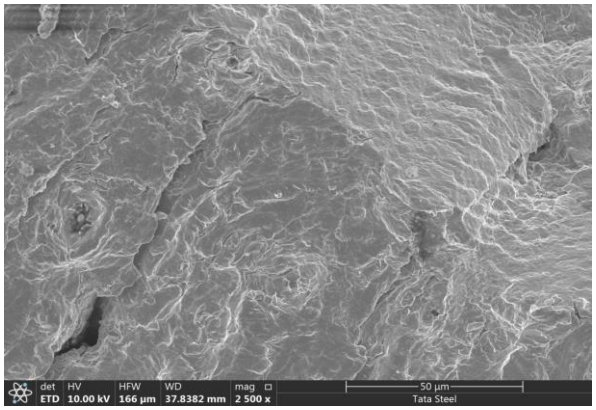

Fig. 10. Crack propagation zone of the 120S AW (N = 639980, Δσ = 380 MPa) specimen

The complete specimen hardness maps for welds of both filler wires were generated and are shown in figure 12. It shows that the results of two passes of welding widens the HAZ from the root side and decreases the minimum hardness of the specimens, making root side more prone to the critical softening. When comparing the hardness maps with DIC measurements and fatigue failure results; In AW conditions, the specimens are failing from high concentration domain at weld and HAZ interface, whereas in WR conditions, 120S and 70S are failing from the domain of minimum hardness at recrystallized HAZ and weld zone, respectively.

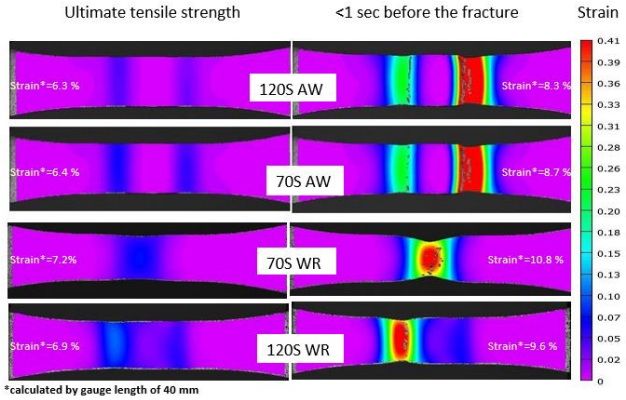

Fig. 11. Results of DIC-measurements for each welding condition

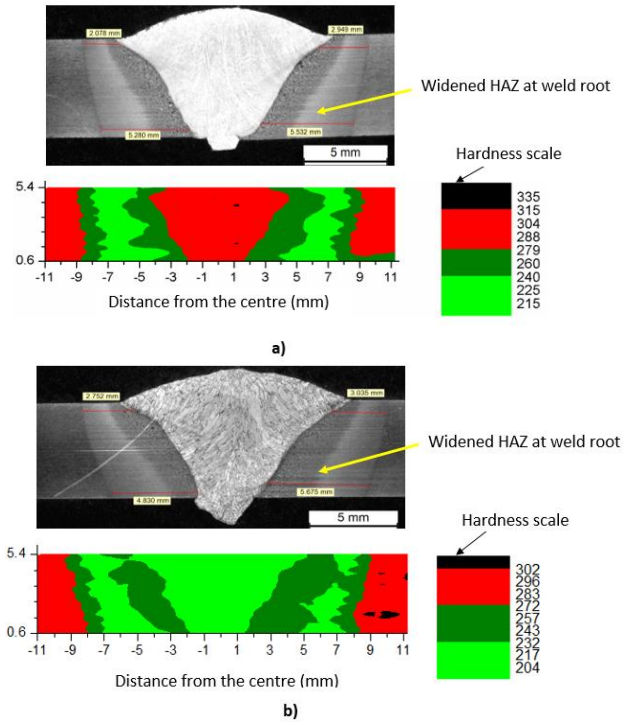

Fig. 12. Hardness maps for, a) 120S welded specimen, b) 70S welded specimen

8. Conclusion

Four welding conditions of GMA welding with two different filler wires and the base material of 700 MPa high strength steel were investigated in this fatigue study: i) 120S AW; ii) 70S

AW; iii) 70S WR; iv) 120S WR; v) BM.

- The combined results of the fatigue analysis, tensile tests with DIC measurements and hardness maps revealed that hardness gradient and the geometrical features are the main controlling factors of the fatigue properties.
- In AW conditions, stress concentration at the weld toe is the main factor responsible for the fatigue strength decrease irrespective of the strength of filler wire used.
- In WR conditions, domain of minimum hardness is the most problematic region. For filler wire having less strength than BM, weld region is mostly prone to the fatigue failure.
- The removing of weld overfill by grinding promotes a significant improvement of the fatigue resistance in comparison with the as welded conditions, as it provides higher crack initiation time.
- Fatigue crack initiation is commonly observed at the face side in AW conditions due to the higher stress concentration and at the root side in WR conditions due to the widening of HAZ leading significant decrease in minimum hardness of the specimen.
- The fatigue resistance of all the welds is lower than the base material as all welds have less crack initiation time than the base material.

Acknowledgement

This work was supported by Tata Steel Limited, Jamshedpur, India. I completed all experimental work at TSL, working as vocational trainee under guidance of Dr. K. S. Arora.

References

[1] Fukumoto, Y. New constructional steels and structural stability, Engineering Structures 1996;786:18-10.
[2] Nishioka K, Ichikawa K. Progress in thermomechanical control of steel plates and their commercialization. Sci. Technol. Adv. Mater 2012;13(2):20.
[3] Callister Jr W. Materials science and engineering an introduction. Seventh edition John Wiley & Sons Inc; 2007.
[4] Infante V, Braga DFO, Duarte F, Moreira PMG, De Freitas M, De Castro PMST. Study of the fatigue behaviour of dissimilar aluminium joints produced by friction stir welding. Int J Fatigue 2016;82:310–6.
[5] Pollard B, Cover R. Fatigue of steel weldments. Weld J American Weld Soc 1972;51(11):544–54.
[6] Vidal C, Infante V. Fatigue behavior of friction stir-welded joints repaired by grinding. J Mater Eng Perform 2014;23(4):1340–9.
[7] Sperle J, Nilsson T. The application of high strength steel for fatigue loaded structures. Proc. HSLA Steels Conf. on Processing, Properties and Applications, Beijing. 1992.
[8] Vidal C, Infante V. Optimization of FS welding parameters for improving mechanical behavior of AA2024-T351 joints based on taguchi method. J Mater Eng Perform 2013;22(8):2261–70.
[9] Dobrovsky Ľ, Dobrovska J. Origination of titanium nitride in a low-carbon steel. Acta Metallurgica Slovaca 1992;2:86–92.
[10] R. Baptista, V. Infante, and C.M. Branco, Study of the Fatigue Behavior in Welded Joints of Stainless Steels Treated by Weld Toe Grinding and Subjected to Salt Water Corrosion, Int. J. Fatigue, 2008, 30, pp. 453–462.
[11] ISO 5817, Welding — Fusion-welded joints in steel, nickel, titanium and their alloys (beam welding excluded) — Quality levels for imperfections, 2014; ISO 5817:2014[E].
[12] “E 739 – 10, Standard Practice for Statistical Analysis of Linearized Stress-Life (S-N) and Strain-Life (ε-N) Fatigue Data,” ASTM International, 2015.